

# 000 PRISM: PARTIAL-LABEL RELATIONAL INFERENCE 001 002 WITH SPATIAL AND SPECTRAL CUES 003 004

005 **Anonymous authors**

006 Paper under double-blind review

## 007 008 ABSTRACT 009

011 In many real-world scenarios, precisely labeling graph data is costly or impractical,  
012 especially in domains like molecular biology or social networks, where  
013 annotation requires expert effort. This challenge motivates partial-label graph  
014 learning, where each graph is weakly annotated with a candidate label set con-  
015 taining the true label. However, such ambiguous supervision makes it hard to  
016 extract reliable semantics and increases the risk of overfitting to noisy candidates.  
017 To address these challenges, we propose PRISM, a unified framework that per-  
018 forms relational inference with spatial and spectral cues to resolve label ambi-  
019 guity. PRISM captures discriminative spatial cues by aligning prototype-guided  
020 substructures across graphs and extracts global spectral cues by decomposing  
021 graph signals into multiple frequency bands with attention, preserving frequency-  
022 specific semantics. These complementary views are integrated into a hybrid re-  
023 lational graph, which supports confidence-aware label propagation under candi-  
024 date constraints. A closed-loop refinement mechanism further stabilizes super-  
025 vision via masked updates and momentum-based confidence estimation. Exten-  
026 sive experiments across diverse benchmarks demonstrate that PRISM consistently  
027 outperforms strong baselines under various noise settings, establishing a new  
028 paradigm for weakly supervised graph classification. The source code is avail-  
029 able at <https://anonymous.4open.science/r/PRISM-17107/>.

## 030 1 INTRODUCTION 031

032 Graph-structured data is pervasive across diverse domains such as drug discovery, molecular prop-  
033 erty prediction, social network analysis, and recommendation systems (Fang et al., 2022; Zhang  
034 et al., 2021b; Wang et al., 2021). These data are naturally represented as graphs, where nodes de-  
035 note entities and edges model relations. To handle such complex structures, Graph Neural Networks  
036 (GNNs) (Welling & Kipf, 2016; Hamilton et al., 2017; Xu et al., 2018; Zhang et al., 2021a) have  
037 emerged as powerful tools for learning expressive graph-level representations, achieving state-of-  
038 the-art results in a wide range of applications including biomedical classification (Liu et al., 2023),  
039 cross-modal retrieval (Chen et al., 2022), and event understanding (Du et al., 2023). GNNs typically  
040 operate by recursively aggregating information from node neighborhoods and summarizing node  
041 embeddings via global pooling (Gao & Ji, 2019; Lee et al., 2021), followed by classification.

042 Despite these advances, existing GNN-based graph classification frameworks are fundamentally  
043 data-intensive: they require accurate and fully labeled training samples to learn discriminative rep-  
044 resentations (Li et al., 2022; Rousseau et al., 2015). However, in many real-world scenarios, ac-  
045 quiring ground-truth labels is prohibitively expensive or technically infeasible. For instance, an-  
046 notating molecular graphs often depends on density functional theory (DFT) simulations (Becke,  
047 2014), which are computationally demanding; in social or biomedical networks, labeling requires  
048 domain experts to manually verify latent properties such as toxicity, protein function, or commu-  
049 nity membership (Yu et al., 2015a). As a result, datasets in practice are often weakly supervised,  
050 with only partial or ambiguous label information available. While self-supervised methods such as  
051 GraphCL (You et al., 2020) alleviate reliance on labels during pre-training by leveraging contrastive  
052 objectives, they still depend on accurate annotations during fine-tuning or evaluation stages. In the  
053 presence of label ambiguity, their performance tends to degrade significantly due to misaligned su-  
pervision signals. This raises a crucial question: *how can we train reliable GNN classifiers in the  
presence of incomplete or uncertain supervision?*

We focus on a practical yet underexplored setting: Partial-label Graph Learning (PLGL). Each graph is annotated with a candidate label set  $\mathcal{S}_i \subset \mathcal{Y}$  containing the true class label, but the exact ground-truth is unknown. This situation commonly arises when annotations are generated from noisy heuristics, coarse rules, or automated labeling tools (Ge et al., 2022). While similar ideas have been studied in image classification (Feng & An, 2019; Lyu et al., 2020), PLGL presents unique challenges due to the structural complexity and non-Euclidean nature of graphs. First, ambiguous supervision introduces semantic uncertainty, making it difficult to capture class-discriminative substructures. Second, standard GNNs tend to overfit noisy signals without precise feedback, particularly when candidate sets contain semantically similar labels. Third, unlike images, graphs exhibit patterns at multiple structural resolutions, from local motifs to global topology, which cannot be represented by uniform pooling or global averaging. Recent works have explored weakly supervised graph classification using pseudo-labeling (Ju et al., 2023) or contrastive learning (You et al., 2020; Luo et al., 2023), but they often face two limitations: (i) reliance on single-view or overconfident predictions, leading to error accumulation and limited robustness under severe ambiguity; and (ii) lack of explicit use of structural and spectral diversity to disentangle candidate labels.

To bridge this gap, we introduce PRISM, a unified and theoretically grounded framework for Partial-label Relational Inference with Spatial and Spectral Modeling. PRISM tackles label ambiguity through three synergistic and mutually reinforcing perspectives. First, it extracts *spatial cues* by aligning prototype-guided substructures across graphs, thereby uncovering class-discriminative local patterns even under noisy candidate sets. Second, it encodes *spectral cues* by decomposing graph signals into multiple frequency bands, where a dedicated multi-band attention mechanism preserves frequency-specific semantics critical for fine-grained reasoning and global structural understanding. Third, it constructs a *hybrid relational graph* that integrates both spatial and spectral similarities, enabling confidence-aware label propagation to refine supervision signals iteratively and coherently. A momentum-based update of soft labels under candidate constraints forms a closed-loop refinement mechanism, which stabilizes training, suppresses noise accumulation, and ultimately yields robust and reliable optimization under weak supervision.

Our contributions are summarized as follows. (1) **Underexplored Problem.** We study the underexplored problem of partial-label graph learning, motivated by practical scenarios with ambiguous supervision in molecular, social, and multimedia domains. (2) **Novel Framework.** We propose PRISM, a novel relational inference framework that integrates spatial and spectral cues to disambiguate labels, combining substructure alignment, frequency-aware encoding, and dual-relational propagation. (3) **Extensive experiments.** We validate PRISM across diverse benchmarks and demonstrate its superiority over existing weakly supervised and graph learning approaches.

## 2 BACKGROUND

**Problem Definition.** Let  $\mathcal{G} = \{G_i = (\mathcal{V}_i, \mathcal{E}_i, \mathbf{X}_i)\}_{i=1}^N$  denote a collection of  $N$  graphs, where each graph  $G_i$  consists of a node set  $\mathcal{V}_i$ , edge set  $\mathcal{E}_i$ , and node features  $\mathbf{X}_i \in \mathbb{R}^{|\mathcal{V}_i| \times d}$ . We denote by  $\mathbf{A}_i \in \{0, 1\}^{|\mathcal{V}_i| \times |\mathcal{V}_i|}$  the adjacency matrix of  $\mathcal{E}_i$ . For each graph  $G_i$ , we are given a candidate label set  $\mathcal{S}_i \subset \mathcal{Y}$ , where  $\mathcal{Y} = \{1, 2, \dots, C\}$  is the complete label space. The candidate set  $\mathcal{S}_i$  includes the true label  $y_i^*$  but does not reveal which one is correct. Our objective is to learn a graph classifier  $f(G_i; \theta)$  that predicts the ground-truth label  $y_i^*$  for each graph in the test set, by training only on ambiguous candidate sets without access to ground-truth supervision.

**Graph Neural Networks.** Graph Neural Networks (GNNs) are widely used to encode graph structures by recursively aggregating information from node neighborhoods. At each layer  $l$ , the representation of node  $v$  is updated by combining its own embedding with messages from its neighbors:

$$\mathbf{h}_v^{(l)} = \phi^{(l)} \left( \mathbf{h}_v^{(l-1)}, \sum_{u \in \mathcal{N}(v)} \psi^{(l)} \left( \mathbf{h}_u^{(l-1)} \right) \right), \quad (1)$$

where  $\phi^{(l)}$  and  $\psi^{(l)}$  are learnable functions, and  $\mathcal{N}(v)$  denotes the neighbor set of node  $v$ .

After  $L$  layers, node embeddings  $\mathbf{h}_v^{(L)}$  are aggregated into a graph-level representation using a read-out function:

$$\mathbf{g} = \text{READOUT} \left( \{\mathbf{h}_v^{(L)}\}_{v \in \mathcal{V}} \right), \quad (2)$$

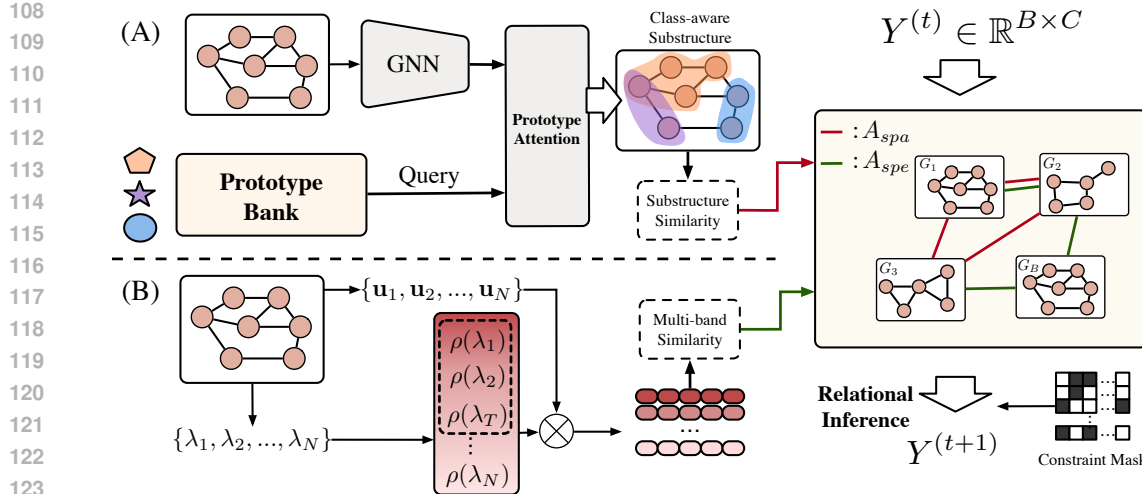


Figure 1: Overview of PRISM. Our framework jointly models spatial substructures (A) and spectral frequency patterns (B) to disambiguate partial labels. Prototype-guided attention and multi-band spectral encoding construct two relational graphs ( $A^{spa}$ ,  $A^{spe}$ ) for iterative label refinement under candidate constraints.

where READOUT can be sum, mean, or attention-based pooling. These graph representations provide the basis for downstream tasks such as graph-level classification.

### 3 METHODOLOGY

This paper introduces a novel framework PRISM for partial-label graph learning that integrates local substructural cues and global spectral dynamics to resolve candidate label ambiguities. Each graph is simultaneously encoded through two complementary pathways: a spatial encoder emphasizes discriminative regions by aligning interpretable subgraphs with label prototypes, while a spectral encoder decomposes graph signals into distinct frequency bands, capturing both smooth and irregular structural patterns. These dual perspectives induce a relational graph with two types of edges: one encoding prototype-based substructure similarity, the other reflecting spectral affinity across graphs. To refine label supervision, we perform confidence-aware propagation over this hybrid graph, fusing signals from both relational types. This design enables the model to distill consistent label cues from noisy candidates, without relying on ground-truth labels. The overview of the proposed framework PRISM is illustrated in Figure 1, and we will elaborate on the details below.

#### 3.1 SPATIAL CUES VIA SUBSTRUCTURE MATCHING

In partial-label graph learning, the true label of each sample is concealed within a noisy candidate set, where multiple labels may be semantically correlated. Relying solely on global representations often blurs these distinctions, since graphs with overlapping candidate labels can exhibit similar overall topology. In contrast, local substructures frequently encode the most discriminative evidence for class separation. Motivated by this observation, we design a structure-aware disambiguation module that aligns interpretable subgraph-level components across related instances, enabling prototype-guided reasoning to uncover consistent label semantics under ambiguity.

To incorporate class-level semantic priors, we maintain a momentum-updated *prototype bank*  $\{p_c \in \mathbb{R}^F\}_{c \in \mathcal{Y}}$ , where each prototype  $p_c$  tracks the aggregated global representation of graphs associated with candidate label  $c$ . At training step  $t$ , we update each prototype as:

$$p_c^{(t)} \leftarrow m \cdot p_c^{(t-1)} + (1 - m) \cdot \frac{1}{|\mathcal{B}_c|} \sum_{i \in \mathcal{B}_c} g_i, \quad (3)$$

where  $g_i = \text{READOUT}(\{h_v^{(L)}\}_{v \in \mathcal{V}_i})$  denotes the global embedding of graph  $G_i$ , and  $\mathcal{B}_c$  is the set of current-batch graphs containing label  $c$  in their candidate set and passing confidence-based filter-

162 ing. Based on the prototype bank, we apply a *prototype-guided attention mechanism* to extract  $C$   
 163 substructure embeddings per graph, where each embedding is aligned with a candidate class. Given  
 164 the node embeddings from the final GNN layer  $\{\mathbf{h}_v^{(L)}\}_{v \in \mathcal{V}_i}$  and the full prototype set  $\{\mathbf{p}_c\}_{c=1}^C$ ,  
 165 attention weights are computed to obtain class-aware latent components:  
 166

$$167 \quad \mathbf{r}_i^{(c)} = \sum_{v \in \mathcal{V}_i} \alpha_{vc} \cdot \mathbf{h}_v^{(L)}, \text{ where } \alpha_{vc} = \frac{\exp(\mathbf{h}_v^{(L)\top} \mathbf{p}_c)}{\sum_{v'} \exp(\mathbf{h}_{v'}^{(L)\top} \mathbf{p}_c)}. \quad (4)$$

170 The resulting embeddings  $\{\mathbf{r}_i^{(c)}\}_{c=1}^C$  serve as interpretable, class-specific substructures for down-  
 171 stream comparison. We then construct a relational graph over graph pairs that share at least one  
 172 candidate label. Let  $\mathcal{P} = \{(i, j) \mid \mathcal{S}_i \cap \mathcal{S}_j \neq \emptyset, i \neq j\}$  denote the set of such graph pairs. For each  
 173 pair  $(G_i, G_j) \in \mathcal{P}$ , we define a prototype-aware substructure similarity:  
 174

$$175 \quad s_{ij}^{spa} = \max_{c \in \mathcal{S}_i \cap \mathcal{S}_j} \cos(\mathbf{r}_i^{(c)}, \mathbf{r}_j^{(c)}) \cdot \cos\left(\frac{\mathbf{r}_i^{(c)} + \mathbf{r}_j^{(c)}}{2}, \mathbf{p}_c\right). \quad (5)$$

178 For each graph, we retain its top- $k_a$  neighbors with the highest  $s_{ij}^{spa}$  scores to form a sparse relational  
 179 graph with a normalized adjacency matrix  $\mathbf{A}^{spa}$  that encodes substructure-level agreement under  
 180 label semantics. This spatial reasoning module provides a fine-grained structural prior, thereby  
 181 enhancing label disambiguation by promoting relational consistency among structurally aligned and  
 182 semantically plausible graph instances across diverse scenarios.  
 183

### 3.2 SPECTRAL CUES VIA MULTI-BAND FREQUENCY ATTENTION

185 While the spatial disambiguation module focuses on extracting local spatial cues, graph spectra  
 186 offer a complementary global perspective by capturing both low-frequency smoothness and high-  
 187 frequency irregularities. However, many existing spectral methods treat all frequency components  
 188 equally, applying uniform aggregation across the spectrum. This equal weighting tends to blur  
 189 structurally diverse signals and may obscure frequency-specific patterns that are crucial for fine-  
 190 grained graph understanding. In contrast, we propose a *Multi-Band Frequency Attention* module that  
 191 not only integrates spectral information into a unified representation but also preserves frequency-  
 192 specific characteristics through explicit band-wise modeling. Specifically, our method: (1) main-  
 193 tains the resolution of each frequency band by employing independently parameterized encoders,  
 194 and (2) supports fine-grained cross-graph reasoning via band-level similarity comparison. This de-  
 195 sign enables frequency-aware graph embeddings that emphasize informative spectral patterns while  
 196 suppressing noise from less relevant bands.  
 197

Given a graph  $G = (\mathcal{V}, \mathcal{E})$  with normalized Laplacian eigenvalues  $\{\lambda_1, \lambda_2, \dots, \lambda_N\}$  and corre-  
 198 sponding eigenvectors  $\{\mathbf{u}_1, \mathbf{u}_2, \dots, \mathbf{u}_N\}$ , we first lift scalar spectral values into a learnable signal  
 199 space using harmonic expansion:

$$200 \quad \rho(\lambda) = [\sin(k\lambda), \cos(k\lambda)]_{k=1}^T \cdot \mathbf{W}_\rho, \quad \rho(\lambda) \in \mathbb{R}^d, \quad (6)$$

202 where  $\mathbf{W}_\rho \in \mathbb{R}^{2T \times d}$  is a shared learnable projection matrix. This produces  $T$  distinct frequency  
 203 embeddings, each serving as a filtered spectral descriptor of the graph. To construct band-specific  
 204 node representations, we modulate the  $p$ -th eigenvector  $\mathbf{u}_p \in \mathbb{R}^N$  with its associated harmonic  
 205 encoding  $\rho(\lambda_p)$  to form:  
 206

$$\mathbf{X}^{(p)} = \mathbf{u}_p \otimes \rho(\lambda_p) \in \mathbb{R}^{N \times d}, \quad (7)$$

207 where  $\otimes$  denotes the outer product broadcast across all nodes. Each  $\mathbf{X}^{(p)}$  is then processed by an  
 208 independently parameterized feedforward network (MLP), resulting in transformed node features  
 209  $\tilde{\mathbf{X}}^{(p)} \in \mathbb{R}^{N \times d}$  that encode frequency-specific semantics. We then apply a message passing neural  
 210 network  $f_{\text{shared}}$ , shared across all frequency bands, to each  $\tilde{\mathbf{X}}^{(p)}$  to extract high-level structural  
 211 signals. For each band  $p \in \{1, \dots, T\}$ , we compute the corresponding graph-level embedding as:  
 212

$$213 \quad \mathbf{z}^{(p)} = \text{READOUT}\left(f_{\text{shared}}(\tilde{\mathbf{X}}^{(p)}, \mathbf{A})\right), \quad (8)$$

215 where  $\mathbf{A}$  denotes the adjacency matrix of the graph. This yields a set of band-level embeddings  
 $\{\mathbf{z}^{(1)}, \dots, \mathbf{z}^{(T)}\}$  that capture structurally filtered representations of the graph across multiple fre-

216 quency perspectives. To synthesize multi-scale structural signals, we employ a soft attention mech-  
 217 anism across bands:

$$219 \quad \mathbf{z} = \sum_{p=1}^T \alpha^{(p)} \mathbf{z}^{(p)}, \text{ where } \alpha^{(p)} = \frac{\exp(\mathbf{a}^\top \sigma(\mathbf{W} \mathbf{z}^{(p)}))}{\sum_{q=1}^T \exp(\mathbf{a}^\top \sigma(\mathbf{W} \mathbf{z}^{(q)}))}. \quad (9)$$

222 Here,  $\mathbf{W}$  and  $\mathbf{a}$  are learnable parameters, and  $\sigma(\cdot)$  denotes a nonlinear activation. For cross-graph  
 223 structural reasoning, we compute band-wise similarity between graphs. Let  $G_i$  and  $G_j$  denote two  
 224 graphs with band embeddings  $\{\mathbf{z}_i^{(p)}\}_{p=1}^T$  and  $\{\mathbf{z}_j^{(p)}\}_{p=1}^T$ , respectively. Their similarity is defined as:

$$226 \quad s_{ij}^{spe} = \max_{p \in \{1, \dots, T\}} \cos(\mathbf{z}_i^{(p)}, \mathbf{z}_j^{(p)}). \quad (10)$$

228 To ensure label-aware alignment, we restrict edges to graph pairs with overlapping candidate sets,  
 229 i.e.,  $\mathcal{S}_i \cap \mathcal{S}_j \neq \emptyset$ . Each graph links to its top- $k_e$  most similar neighbors, forming a relational graph  
 230 with normalized adjacency matrix  $\mathbf{A}^{spe}$  that supports label disambiguation.

231 We theoretically establish that both  $\mathbf{A}^{spa}$  and  $\mathbf{A}^{spe}$  contribute to label disambiguation. Intuitively,  
 232 the distribution of hidden node embeddings should be determined by the prototype of the true label  
 233 to a certain degree. Building on this observation, we present the following theorem with proof  
 234 provided in Appendix A:

236 **Theorem 1.** Assume  $\mathbb{E}[h_v^{(i)} | y_i^* = c] = p_c$ ,  $\forall v \in \mathcal{V}_i$ ,  $\eta_{jk}^{(i)} = \mathbb{P}(\mathbf{A}_i(j, k) = 1)$  is random variable  
 237 whose distribution can be determined by  $y_i^*$ , and  $\min_{1 \leq i \leq N, 1 \leq p \leq T} |\lambda_{p+1}^{(i)} - \lambda_p^{(i)}| \geq \delta$  for some  
 238  $\delta > 0$ . Then, we have for any  $i, j \in \{1, 2, \dots, N\}$ :

$$240 \quad \mathbb{P}(A_{ij}^{spa} = 1 | y_i^* = y_j^*) \rightarrow 1 \quad (11)$$

242 and

$$243 \quad \mathbb{P}(A_{ij}^{spe} = 1 | y_i^* = y_j^*) \rightarrow 1 \quad (12)$$

244 as  $|\mathcal{V}_i|, |\mathcal{V}_j| \rightarrow \infty$ .

245 Theorem 1 suggests that if graph  $i$  and  $j$  shares the same true label, the probabilities of  $A_{ij}^{spa}$  and  
 246  $A_{ij}^{spe}$  being 1 will both converge to 1, which works on the subsequent label propagation with disam-  
 247 biguation from noisy candidate sets.

### 250 3.3 LABEL DISAMBIGUATION VIA RELATIONAL INFERENCE

251 Based on the relational graph constructed in previous modules, which encodes spatial proximity and  
 252 spectral correlation as distinct relational types, we develop an iterative label propagation framework  
 253 to enhance supervision under partially labeled settings where ground-truth labels are inaccessible.  
 254 This framework integrates complementary structural and spectral signals, progressively refining soft  
 255 supervision, while rigorously enforcing candidate label constraints throughout the entire refinement  
 256 process to ensure both semantic validity and training stability.

257 Let  $\mathbf{Y}^{(0)} \in \mathbb{R}^{N \times C}$  denote the initial soft label matrix, where  $N$  is the number of graphs and  $C$  the  
 258 number of classes. At each iteration  $t$ , label signals are updated using two normalized adjacency  
 259 matrices:  $\mathbf{A}^{spa}$  for spatial relations and  $\mathbf{A}^{spe}$  for spectral affinity. The propagation rule is:

$$261 \quad \tilde{\mathbf{Y}}^{(t+1)} = \alpha \cdot \mathbf{Y}^{(t)} + (1 - \alpha) \cdot \mathcal{N}(\mathbf{A}^{spa} \mathbf{Y}^{(t)} + \mathbf{A}^{spe} \mathbf{Y}^{(t)}), \quad (13)$$

263 where  $\alpha \in (0, 1)$  controls the update momentum, and  $\mathcal{N}(\cdot)$  denotes row-wise  $\ell_1$  normalization. To  
 264 constrain label propagation to valid candidate classes, we apply a binary mask  $\mathbf{M} \in \{0, 1\}^{N \times C}$   
 265 after each update:

$$266 \quad \mathbf{Y}^{(t+1)} = \mathcal{N}(\tilde{\mathbf{Y}}^{(t+1)} \odot \mathbf{M}), \quad (14)$$

268 where  $\odot$  denotes element-wise multiplication. After  $T$  iterations, the refined label matrix  $\mathbf{Y}^{(T)}$  cap-  
 269 tures multi-relational consistency while remaining faithful to partial supervision, enabling effective  
 270 disambiguation of noisy candidate sets. We maintain a soft label confidence matrix  $\mathbf{Q} \in \mathbb{R}^{N \times C}$ ,

270 initialized uniformly over candidate classes. To adaptively improve supervision quality,  $\mathbf{Q}$  is  
 271 periodically updated using the soft labels  $\mathbf{Y}^{(T)}$  inferred through relational propagation. The update  
 272 follows an exponential moving average (EMA) scheme:  
 273

$$\mathbf{Q}_i \leftarrow \mathcal{N} \left( m \cdot \mathbf{Q}_i + (1 - m) \cdot \mathbf{Y}_i^{(T)} \right), \quad (15)$$

275 where  $m \in (0, 1)$  is the momentum coefficient and  $\mathcal{N}(\cdot)$  denotes row-wise  $\ell_1$  normalization applied  
 276 over candidate entries. This closed-loop mechanism ensures alignment between model predictions  
 277 and structure-aware label signals, promoting stable and reliable supervision during training.  
 278

### 279 3.4 UNIFIED TRAINING OBJECTIVE

280 To train the model under partial supervision, we adopt a unified objective that couples candidate-  
 281 constrained loss with confidence-aware refinement. The final predictions are obtained by applying  
 282 an MLP-based classifier to the spatial-view embeddings  $\mathbf{g}$ , producing logits  $\mathbf{P}^{spa} \in \mathbb{R}^{N \times C}$ . In  
 283 parallel, a distinct classifier processes the spectral-view embeddings  $\mathbf{z}$  to yield  $\mathbf{P}^{spe} \in \mathbb{R}^{N \times C}$ . The  
 284 training loss for the spatial (spectral) view is defined as the negative marginal log-likelihood over  
 285 candidate classes:  
 286

$$\mathcal{L}_{sup}^{(o)} = -\frac{1}{B} \sum_{i=1}^B \log \sum_{c \in \mathcal{S}_i} \text{Softmax}(\mathbf{P}_i^{(o)})_c \cdot \mathbf{Q}_{ic}, \quad o \in \{spa, spe\}, \quad (16)$$

287 where  $\mathcal{S}_i$  is the candidate label set for sample  $i$ , and  $B$  is the batch size. This formulation encourages  
 288 the model to align predictions with the confidence-weighted support within each candidate set. We  
 289 jointly optimize the spatial and spectral objectives to extract complementary supervisory signals:  
 290

$$\mathcal{L} = \mathcal{L}_{sup}^{spa} + \mathcal{L}_{sup}^{spe}, \quad (17)$$

291 This dual-view supervision facilitates robust label disambiguation under uncertainty. We then offer  
 292 a theoretical analysis of the proposed method, particularly focusing on the convergence of the label  
 293 confidence matrix and training loss under certain conditions. To begin with, let  $\mathbf{Y}^* = (Y_i^*)_{i=1}^N \in$   
 294  $\{0, 1\}^{N \times C}$  be the matrix consisting of ground-truth one-hot label vector. Denote the classifier as  
 295  $f_{classifier}$  which produces partial label confidence matrix  $P$ , the final predicted label confidence  
 296 vector of graph  $i$  is  $\mathbf{P}_i = f_{classifier}(\mathbf{g}_i)$ . If the classifier is well-trained, it should recover label  $c$   
 297 from  $p_c$  since  $p_c$  is the prototype of label  $c$ . Based on this, we have the following results with the  
 298 proof in Appendix B:  
 299

300 **Theorem 2.** *Under the assumption of Theorem 1, further assume  $f_{classifier}(p_c) = \mathbb{I}_c$ ,  $\forall c \in \mathcal{Y}$   
 301 where  $\mathbb{I}_c \in \{0, 1\}^C$  denotes one-hot vector whose  $c$ -th component is 1 while the rest are 0, we have:*

$$\mathbf{Q}_i \xrightarrow{a.s.} \mathbf{Y}_i^* \quad (18)$$

302 as  $|\mathcal{V}_i|, T \rightarrow \infty$ . And

$$\mathbb{E} [\mathcal{L}_{sup}] \rightarrow 0 \quad (19)$$

303 as  $\min_{1 \leq i \leq N} |\mathcal{V}_i|, T \rightarrow \infty$ .

304 Theorem 2 indicates that if each graph has enough node information and we iterate enough epochs,  
 305 the soft label confidence matrix updated by EMA will converge to the ground-truth and training  
 306 loss will tend to zero, which further implies our framework can resolve label ambiguity by aligning  
 307 prototype-guided substructures across graphs. The condition  $|\mathcal{V}_i| \rightarrow \infty$  can be replaced by  $B, N \rightarrow$   
 308  $\infty$  to a certain degree, since graphs with the same label and candidate label set can be regarded as a  
 309 whole, and the whole number of nodes tends to infinity when  $B, N \rightarrow \infty$ .  
 310

### 311 3.5 COMPUTATIONAL EFFICIENCY ANALYSIS

312 Let  $N$  be the number of nodes,  $|\mathcal{E}|$  the number of edges,  $d$  the feature dimension,  $L$  the number  
 313 of GNN layers, and  $T$  the number of spectral bands. In preprocessing, we compute the  $k$  smallest  
 314 eigenvectors and their spectral encodings, which are reused throughout training. During training, the  
 315 spatial view performs message passing with complexity  $\mathcal{O}(L|\mathcal{E}|d)$ , while the spectral view operates  
 316 on pre-computed features across  $T$  bands and applies shared MLPs, resulting in a total cost of  
 317  $\mathcal{O}(TNd)$ . Since  $L$  and  $T$  are small constants, the overall training complexity is  $\mathcal{O}(|\mathcal{E}|d)$ , which is  
 318 linear in the number of edges and consistent with standard GNN-based methods.

324  
 325 Table 1: The classification accuracy (mean% $\pm$ std%) on five graph benchmark datasets. The best  
 326 results are shown in boldface and the second best results are underlined.  $q = P(\bar{y} \in Y | \bar{y} \neq y)$   
 327 reflecting the degree of label ambiguity.

Datasets	ENZYMES		Letter-High		COIL-DEL		CIFAR10		COLORS-3	
Methods	$q = 0.3$	$q = 0.5$	$q = 0.3$	$q = 0.5$	$q = 0.05$	$q = 0.1$	$q = 0.3$	$q = 0.5$	$q = 0.3$	$q = 0.5$
GCN	48.44 $\pm$ 2.06	40.22 $\pm$ 2.93	44.00 $\pm$ 1.08	35.94 $\pm$ 1.82	50.43 $\pm$ 1.07	41.63 $\pm$ 1.74	43.68 $\pm$ 0.68	41.35 $\pm$ 0.65	74.87 $\pm$ 0.25	60.67 $\pm$ 1.64
GAT	49.11 $\pm$ 2.93	34.67 $\pm$ 3.87	61.33 $\pm$ 3.48	53.04 $\pm$ 3.06	59.77 $\pm$ 1.97	46.63 $\pm$ 1.54	52.93 $\pm$ 1.22	48.54 $\pm$ 0.46	71.83 $\pm$ 0.22	62.56 $\pm$ 3.54
GIN	47.11 $\pm$ 4.59	34.22 $\pm$ 1.78	50.43 $\pm$ 1.92	35.59 $\pm$ 3.75	46.23 $\pm$ 0.88	37.29 $\pm$ 1.04	43.91 $\pm$ 0.43	41.24 $\pm$ 0.52	48.17 $\pm$ 0.44	41.00 $\pm$ 2.75
GraphSAGE	47.33 $\pm$ 3.03	39.33 $\pm$ 3.11	70.96 $\pm$ 1.48	60.35 $\pm$ 1.83	58.91 $\pm$ 1.92	49.23 $\pm$ 1.90	51.92 $\pm$ 0.26	47.44 $\pm$ 0.83	71.24 $\pm$ 3.00	56.63 $\pm$ 5.81
TopKPool	44.22 $\pm$ 2.76	36.00 $\pm$ 4.80	55.25 $\pm$ 2.74	43.83 $\pm$ 5.21	44.83 $\pm$ 2.19	34.63 $\pm$ 2.08	48.97 $\pm$ 1.24	42.87 $\pm$ 1.31	56.69 $\pm$ 3.58	33.49 $\pm$ 1.74
SAGPool	46.67 $\pm$ 2.53	37.11 $\pm$ 5.00	55.71 $\pm$ 4.71	39.30 $\pm$ 5.49	41.89 $\pm$ 4.28	30.17 $\pm$ 1.85	50.01 $\pm$ 0.68	45.16 $\pm$ 0.36	59.91 $\pm$ 4.14	24.62 $\pm$ 0.32
EdgePool	51.11 $\pm$ 3.06	33.33 $\pm$ 1.99	64.17 $\pm$ 2.44	55.36 $\pm$ 2.16	56.74 $\pm$ 3.98	45.89 $\pm$ 1.30	50.17 $\pm$ 0.64	45.90 $\pm$ 0.44	76.96 $\pm$ 0.13	62.31 $\pm$ 1.23
ASAP	44.44 $\pm$ 3.06	31.56 $\pm$ 3.34	65.04 $\pm$ 1.22	52.75 $\pm$ 4.41	46.20 $\pm$ 4.08	34.94 $\pm$ 3.02	50.10 $\pm$ 0.63	44.81 $\pm$ 1.57	70.11 $\pm$ 0.54	62.47 $\pm$ 0.98
Graph Transplant	51.78 $\pm$ 2.39	43.78 $\pm$ 3.41	74.84 $\pm$ 1.44	66.78 $\pm$ 1.86	66.57 $\pm$ 1.60	57.11 $\pm$ 1.03	53.79 $\pm$ 1.11	48.95 $\pm$ 1.47	74.66 $\pm$ 1.30	62.72 $\pm$ 2.37
PiCO	46.88 $\pm$ 2.76	35.78 $\pm$ 3.02	73.56 $\pm$ 1.71	64.63 $\pm$ 4.35	76.25 $\pm$ 1.66	63.69 $\pm$ 1.42	53.47 $\pm$ 1.14	46.04 $\pm$ 1.20	53.99 $\pm$ 0.92	34.74 $\pm$ 1.77
TGNN	53.33 $\pm$ 3.51	42.22 $\pm$ 4.39	70.43 $\pm$ 0.97	59.83 $\pm$ 1.32	62.28 $\pm$ 1.05	50.20 $\pm$ 1.17	OOM	OOM	75.84 $\pm$ 1.81	63.95 $\pm$ 2.18
GraphCL	54.22 $\pm$ 5.14	39.78 $\pm$ 5.09	72.00 $\pm$ 2.01	62.49 $\pm$ 2.00	69.94 $\pm$ 2.31	60.17 $\pm$ 2.96	53.57 $\pm$ 0.87	48.10 $\pm$ 0.61	72.89 $\pm$ 1.24	61.55 $\pm$ 1.01
GraphACL	54.44 $\pm$ 2.33	44.89 $\pm$ 4.75	69.80 $\pm$ 1.01	57.68 $\pm$ 2.85	71.40 $\pm$ 0.95	60.29 $\pm$ 3.04	53.25 $\pm$ 0.62	47.86 $\pm$ 0.65	73.84 $\pm$ 2.12	63.57 $\pm$ 1.39
DEER	58.22 $\pm$ 2.18	47.56 $\pm$ 2.57	80.12 $\pm$ 1.26	72.29 $\pm$ 1.54	79.94 $\pm$ 1.20	68.03 $\pm$ 1.11	57.08 $\pm$ 0.57	52.48 $\pm$ 0.72	88.13 $\pm$ 2.08	66.81 $\pm$ 2.82
<b>PRISM (Ours)</b>	<b>63.11<math>\pm</math>0.83</b>	<b>51.33<math>\pm</math>3.61</b>	<b>82.55<math>\pm</math>0.89</b>	<b>78.32<math>\pm</math>1.37</b>	<b>85.69<math>\pm</math>1.06</b>	<b>79.48<math>\pm</math>1.45</b>	<b>58.29<math>\pm</math>0.83</b>	<b>55.10<math>\pm</math>0.98</b>	<b>91.93<math>\pm</math>2.26</b>	<b>80.57<math>\pm</math>2.69</b>

## 4 EXPERIMENTS

### 4.1 EXPERIMENTAL SETUP

**Datasets.** To comprehensively assess the performance of PRISM, we conduct experiments on five established graph classification benchmarks spanning the bioinformatics and vision domains: ENZYMES (Schomburg et al., 2004), Letter-High (Riesen & Bunke, 2008), COIL-DEL (Riesen & Bunke, 2008), CIFAR10 (Dwivedi et al., 2020), and COLORS-3 (Knyazev et al., 2019). Following (Gu et al., 2024), we randomly inject false positive labels into the candidate set to generate partial-label data. Specifically, each incorrect label  $\bar{y} \neq y$  is included with probability  $q = P(\bar{y} \in \mathcal{Y} | \bar{y} \neq y)$ , controlling the degree of label ambiguity. A higher  $q$  indicates noisier candidate supervision. We set  $q \in \{0.1, 0.3, 0.5\}$  for most datasets, and  $q \in \{0.02, 0.05, 0.1\}$  for COIL-DEL to account for its larger label space. More details are provided in the Appendix E.

**Baseline Methods.** We compare our proposed PRISM with a comprehensive set of baselines across multiple paradigms: (a) *Graph neural networks*: GCN (Welling & Kipf, 2016), GAT (Veličković et al., 2017), GIN (Xu et al., 2018), and GraphSAGE (Hamilton et al., 2017); (b) *Hierarchical graph pooling methods*: TopKPool (Gao & Ji, 2019), SAGPool (Lee et al., 2019), EdgePool (Diehl, 2019), and ASAP (Ranjan et al., 2020), all using GraphSAGE as the backbone; (c) *Graph augmentation method*: Graph Transplant (Park et al., 2022); (d) *Unsupervised contrastive graph learning*: GraphCL (You et al., 2020) and GraphACL (Luo et al., 2023); (e) *Semi-supervised graph learning*: TGNN (Ju et al., 2023); (f) *Partial label learning in vision*: PiCO (Wang et al., 2022), adapted to the graph setting with a GraphSAGE encoder for fair comparison; (g) *Partial label learning for graphs*: DEER (Gu et al., 2024). Further details on the baselines are provided in the Appendix F.

**Implementation and Evaluation Protocol.** All experiments are implemented using PyTorch with the PyG backend. We use a two-layer GraphSAGE with 512 hidden units as the shared encoder across all models. Training is performed using the Adam optimizer (Kingma & Ba, 2014) with an initial learning rate of 0.001 and a batch size of 128. All reported results are averaged over five independent runs with different random seeds, each reporting mean accuracy and standard deviation. More details about the implementation are provided in the Appendix G.

### 4.2 PERFORMANCE COMPARISON

Table 1 summarizes the classification performance of PRISM against diverse baselines under varying label ambiguity levels ( $q$ ). The results highlight four key findings: (1) PRISM achieves consistently superior performance across all datasets and ambiguity settings, surpassing baselines by a considerable margin. For example, on ENZYMES, our method outperforms the second-best by

378

379

Table 2: Ablation study on ENZYMEs, Letter-High, and CIFAR10.

380

381

382

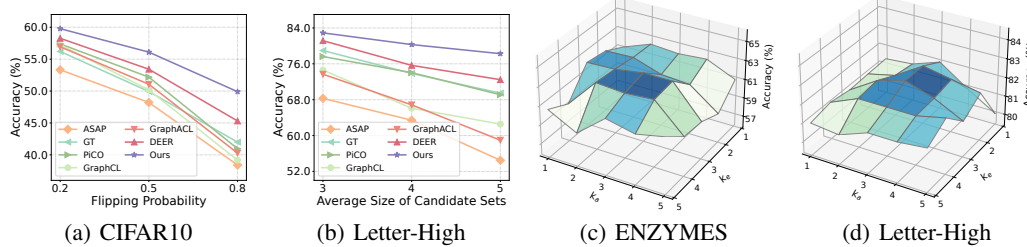
383

384

385

386

Datasets	ENZYMEs		Letter-High		CIFAR10	
Variants	$q = 0.3$	$q = 0.5$	$q = 0.3$	$q = 0.5$	$q = 0.3$	$q = 0.5$
PRISM w/o Sub	$61.78 \pm 2.06$	$49.56 \pm 3.55$	$80.70 \pm 1.20$	$76.11 \pm 2.19$	$56.65 \pm 1.01$	$53.30 \pm 0.77$
PRISM w/o Spa	$60.89 \pm 2.26$	$48.00 \pm 3.87$	$79.65 \pm 1.21$	$74.72 \pm 0.99$	$55.23 \pm 1.19$	$51.72 \pm 1.08$
PRISM w/o Spe	$61.55 \pm 1.94$	$48.89 \pm 2.11$	$80.17 \pm 0.43$	$76.46 \pm 2.45$	$55.72 \pm 0.93$	$52.65 \pm 1.12$
PRISM w/o Rel. Infer	$57.78 \pm 2.81$	$45.11 \pm 3.95$	$78.43 \pm 1.03$	$71.24 \pm 2.18$	$53.61 \pm 1.32$	$49.79 \pm 1.27$
<b>PRISM (Full Model)</b>	<b><math>63.11 \pm 0.83</math></b>	<b><math>51.33 \pm 3.61</math></b>	<b><math>82.55 \pm 0.89</math></b>	<b><math>78.32 \pm 1.37</math></b>	<b><math>58.29 \pm 0.83</math></b>	<b><math>55.10 \pm 0.98</math></b>

Figure 2: (a) Performance comparison in scenarios with hierarchical label noise. (b) Performance comparison in scenarios with competitive label noise. (c)(d) Performance w.r.t. top- $k_a$  and top- $k_e$  on ENZYMEs and Letter-High.

8.3% under  $q = 0.3$ , confirming its robustness and generalization under weak supervision. (2) On fine-grained datasets such as COIL-DEL, where class granularity and semantic ambiguity are pronounced, PRISM retains a strong advantage even at high noise. On COIL-DEL with  $q = 0.1$ , it attains 79.48% accuracy, exceeding the prior best (DEER, 68.03%) by 16.8%, showing effective candidate disambiguation via complementary spectral and substructure cues. (3) Compared to vision-based partial-label methods (e.g., PiCO) and semi-supervised models (e.g., TGNN), our framework consistently improves performance across all graph datasets. Although PiCO with GraphSAGE encoders is adapted to graphs, it still lags, underscoring the limits of directly transferring CV-based methods and the necessity of graph-specific modeling. (4) As label ambiguity  $q$  increases, most methods degrade sharply, whereas PRISM exhibits a much slower decline. This robustness stems from integrating spectral and substructural reasoning, with confidence-aware propagation mitigating noisy and misleading supervision. More results under  $q = 0.1$  are provided in Appendix D.

**Semantically Correlated Label Noise.** In many real-world scenarios, labels are not independent but semantically correlated, leading to candidate sets that contain noisy labels with stronger affinity to the ground-truth than unrelated classes, thereby creating additional challenges for robust learning. This raises the challenge of whether PRISM can reliably address such semantically entangled ambiguity. To evaluate this, we design two experimental protocols: (1) *Hierarchical label noise*. We exploit the coarse-to-fine taxonomy of CIFAR10 (e.g., vehicles vs. animals) and introduce noise by flipping negative labels within the same super-class as the true label with probability  $q$ , thereby forming semantically plausible candidates. (2) *Competitive label noise*. Following (Yan & Guo, 2023), we pretrain a graph neural network (GNN) on clean data to capture inter-class semantic dependencies. We then randomly select noisy candidates from the Top- $K$  predictions of this GNN, with  $K = 6$  for Letter-High, and vary the candidate set size by adjusting sampling ratios. The results, presented in Figure 2 (a)(b), show that PRISM consistently outperforms all baselines under both noise schemes across different ambiguity levels, thereby highlighting its robustness to semantically correlated label noise. Details of the CIFAR10 hierarchy are provided in Appendix E.

#### 4.3 ABLATION STUDY

To assess the contribution of each core component in PRISM, we conduct ablation experiments on ENZYMEs, Letter-High, and CIFAR10 under noise levels  $q = 0.3$  and  $q = 0.5$ , with results in Table 2. Removing substructure alignment (PRISM w/o Sub) and replacing class-specific matching with holistic graph embeddings causes clear performance drops, especially under high ambiguity, showing that discriminative substructure cues outperform coarse comparisons. Excluding the spatial branch (PRISM w/o Spa) further reduces accuracy, as the absence of neighborhood-aware

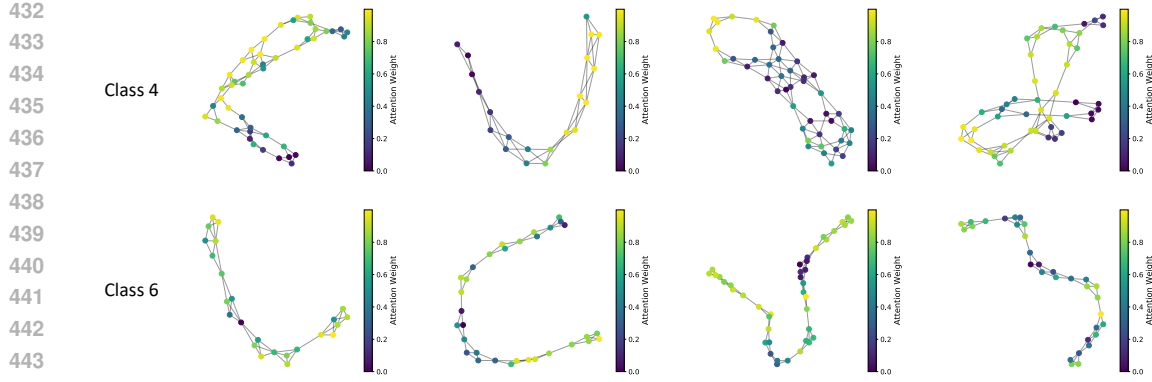


Figure 3: Class-specific attention maps reveal consistent focus on discriminative substructures across graph instances within different categories.

signals weakens the capture of fine-grained topology critical for resolving label ambiguity, particularly in CIFAR10. Discarding the spectral attention module (PRISM w/o Spe) validates the value of frequency-specific reasoning, since multi-band decomposition highlights global semantics complementing local structure. Most critically, removing the relational inference layer (PRISM w/o Rel. Infer) yields the sharpest degradation, especially at  $q = 0.5$ , underscoring that graph-of-graph modeling and label propagation are indispensable for suppressing noise and ensuring robust supervision.

#### 4.4 SENSITIVITY ANALYSIS

To investigate the influence of relational sparsity, we analyze how the number of neighbors retained in the spatial ( $k_a$ ) and spectral ( $k_e$ ) relational graphs affects performance. As illustrated in Figure 2 (c)(d), accuracy generally increases as  $k_a$  and  $k_e$  grow from 1 to moderate values, then saturates or slightly declines. This pattern indicates that adding structurally or spectrally aligned instances improves cross-graph consistency by enhancing the density of reliable signals. However, overly dense connectivity introduces noisy or weakly correlated neighbors, diluting discriminative patterns and potentially causing label propagation drift. Our model achieves stable performance under a broad range of  $k$  values, reflecting robustness to hyperparameter choices in multi-view graph construction.

#### 4.5 VISUALIZATION OF CLASS-SPECIFIC ATTENTION

To assess the interpretability of our spatial encoder, we visualize class-conditioned attention maps from the ENZYME dataset. As shown in Figure 3, each node is colored by its attention weight relative to the ground-truth class prototype, with warmer colors denoting greater contribution to class-specific substructure reasoning. The model consistently highlights structurally informative regions, such as densely connected motifs, central connectors, or bridging nodes, while down-weighting peripheral or less relevant parts of the graph. Despite structural variability across samples, attention patterns remain highly consistent within the same class, indicating that prototype-guided attention effectively identifies semantically aligned substructures relevant for enzyme classification and provides human-interpretable insights into functionally critical topological regions.

## 5 CONCLUSION

In this work, we study the underexplored problem of partial-label graph learning, where each graph is annotated with an ambiguous candidate label set. To address the inherent challenges of semantic uncertainty and structural complexity, we propose PRISM, a unified relational inference framework that integrates spatial substructure alignment and spectral frequency modeling via dual relational graphs. Our method leverages confidence-aware label propagation and candidate-constrained refinement to disambiguate supervision without relying on ground-truth annotations or external auxiliary signals. Extensive experiments across multiple benchmarks validate the effectiveness, robustness, and generalizability of PRISM under various ambiguity levels, highlighting its potential as a principled and versatile solution for learning from weakly supervised graph data.

486 ETHICS STATEMENT  
487488 We acknowledge that all co-authors of this work have read and committed to adhering to the ICLR  
489 Code of Ethics.  
490491 REPRODUCIBILITY STATEMENT  
492493 We have included all details about the datasets and our experiment settings in Appendix E and  
494 Appendix G, respectively. The anonymous source code can be found in <https://anonymous.4open.science/r/PRISM-17107/>. The code and related materials will be appropriately  
495 released to ensure the transparency and reproducibility of our work.  
496497 REFERENCES  
498500 Axel D Becke. Perspective: Fifty years of density-functional theory in chemical physics. *The  
501 Journal of chemical physics*, 140(18):18A301, 2014.  
502503 Deyu Bo, Yuan Fang, Yang Liu, and Chuan Shi. Graph contrastive learning with stable and scalable  
504 spectral encoding. *Advances in Neural Information Processing Systems*, 36:45516–45532, 2023.  
505506 Dapeng Chen, Min Wang, Haobin Chen, Lin Wu, Jing Qin, and Wei Peng. Cross-modal retrieval  
507 with heterogeneous graph embedding. In *Proceedings of the 30th ACM International Conference  
508 on Multimedia*, pp. 3291–3300, 2022.509 Timothee Cour, Ben Sapp, and Ben Taskar. Learning from partial labels. *The Journal of Machine  
510 Learning Research*, 12:1501–1536, 2011.  
511512 Frederik Diehl. Edge contraction pooling for graph neural networks. *arXiv preprint  
513 arXiv:1905.10990*, 2019.  
514515 Zilin Du, Yunxin Li, Xu Guo, Yidan Sun, and Boyang Li. Training multimedia event extraction  
516 with generated images and captions. In *Proceedings of the 31st ACM International Conference  
517 on Multimedia*, pp. 5504–5513, 2023.518 Vijay Prakash Dwivedi, Chaitanya K Joshi, Thomas Laurent, Yoshua Bengio, and Xavier Bresson.  
519 Benchmarking graph neural networks. *arXiv preprint arXiv:2003.00982*, 2020.  
520521 Xiaomin Fang, Lihang Liu, Jieqiong Lei, Donglong He, Shanzhuo Zhang, Jingbo Zhou, Fan Wang,  
522 Hua Wu, and Haifeng Wang. Geometry-enhanced molecular representation learning for property  
523 prediction. *Nature Machine Intelligence*, 4(2):127–134, 2022.  
524525 Lei Feng and Bo An. Partial label learning by semantic difference maximization. In *IJCAI*, pp.  
526 2294–2300, 2019.  
527528 Hang Gao, Jiaguo Yuan, Jiangmeng Li, Peng Qiao, Fengge Wu, Changwen Zheng, and Huaping Liu.  
529 Graph partial label learning with potential cause discovering. *arXiv preprint arXiv:2403.11449*,  
530 2024.  
531532 Hongyang Gao and Shuiwang Ji. Graph u-nets. In *international conference on machine learning*,  
533 pp. 2083–2092. PMLR, 2019.  
534535 Lingchi Ge, Min Fang, Haikun Li, and Bo Chen. Label correlation for partial label learning. *Journal  
536 of Systems Engineering and Electronics*, 33(5):1043–1051, 2022.  
537538 Yiyang Gu, Zihao Chen, Yifang Qin, Zhengyang Mao, Zhiping Xiao, Wei Ju, Chong Chen, Xian-  
539 Sheng Hua, Yifan Wang, Xiao Luo, et al. Deer: Distribution divergence-based graph contrast for  
540 partial label learning on graphs. *IEEE Transactions on Multimedia*, 2024.  
541542 Will Hamilton, Zhitao Ying, and Jure Leskovec. Inductive representation learning on large graphs.  
543 *Advances in neural information processing systems*, 30, 2017.  
544

540 Eyke Hüllermeier and Jürgen Beringer. Learning from ambiguously labeled examples. In *Advances*  
 541 *in Intelligent Data Analysis VI: 6th International Symposium on Intelligent Data Analysis, IDA*  
 542 *2005, Madrid, Spain, September 8-10, 2005. Proceedings 6*, pp. 168–179. Springer, 2005.

543

544 Wei Ju, Xiao Luo, Meng Qu, Yifan Wang, Chong Chen, Minghua Deng, Xian-Sheng Hua, and Ming  
 545 Zhang. Tgnn: A joint semi-supervised framework for graph-level classification. *arXiv preprint*  
 546 *arXiv:2304.11688*, 2023.

547 Diederik P Kingma and Jimmy Ba. Adam: A method for stochastic optimization. *arXiv preprint*  
 548 *arXiv:1412.6980*, 2014.

549

550 Boris Knyazev, Graham W Taylor, and Mohamed Amer. Understanding attention and generalization  
 551 in graph neural networks. *Advances in neural information processing systems*, 32, 2019.

552 Dongha Lee, Su Kim, Seonghyeon Lee, Chanyoung Park, and Hwanjo Yu. Learnable structural  
 553 semantic readout for graph classification. In *2021 IEEE International Conference on Data Mining*  
 554 (*ICDM*), pp. 1180–1185. IEEE, 2021.

555 Junhyun Lee, Inyeop Lee, and Jaewoo Kang. Self-attention graph pooling. In *International confer-*  
 556 *ence on machine learning*, pp. 3734–3743. PMLR, 2019.

557

558 Sihang Li, Xiang Wang, An Zhang, Yingxin Wu, Xiangnan He, and Tat-Seng Chua. Let invariant  
 559 rationale discovery inspire graph contrastive learning. In *International conference on machine*  
 560 *learning*, pp. 13052–13065. PMLR, 2022.

561

562 Meng Liu, Ke Liang, Dayu Hu, Hao Yu, Yue Liu, Lingyuan Meng, Wenxuan Tu, Sihang Zhou, and  
 563 Xinxing Liu. Tmac: Temporal multi-modal graph learning for acoustic event classification. In  
 564 *Proceedings of the 31st ACM International Conference on Multimedia*, pp. 3365–3374, 2023.

565

566 Xiao Luo, Wei Ju, Yiyang Gu, Zhengyang Mao, Luchen Liu, Yuhui Yuan, and Ming Zhang. Self-  
 567 supervised graph-level representation learning with adversarial contrastive learning. *ACM Trans-*  
 568 *actions on Knowledge Discovery from Data*, 18(2):1–23, 2023.

569

570 Gengyu Lyu, Songhe Feng, Tao Wang, and Congyan Lang. A self-paced regularization framework  
 571 for partial-label learning. *IEEE Transactions on Cybernetics*, 52(2):899–911, 2020.

572

573 Mourad Oudghiri. Weyl’s theorem and perturbations. *Integral Equations and Operator Theory*, 53  
 574 (4):535–545, 2005.

575

576 Joonhyung Park, Hajin Shim, and Eunho Yang. Graph transplant: Node saliency-guided graph  
 577 mixup with local structure preservation. In *Proceedings of the AAAI Conference on Artificial*  
 578 *Intelligence*, volume 36, pp. 7966–7974, 2022.

579

580 Ekagra Ranjan, Soumya Sanyal, and Partha Talukdar. Asap: Adaptive structure aware pooling for  
 581 learning hierarchical graph representations. In *Proceedings of the AAAI Conference on Artificial*  
 582 *Intelligence*, volume 34, pp. 5470–5477, 2020.

583

584 Kaspar Riesen and Horst Bunke. Iam graph database repository for graph based pattern recognition  
 585 and machine learning. In *Joint IAPR International Workshops on Statistical Techniques in Pat-*  
 586 *tern Recognition (SPR) and Structural and Syntactic Pattern Recognition (SSPR)*, pp. 287–297.  
 587 Springer, 2008.

588

589 François Rousseau, Emmanouil Kiagias, and Michalis Vazirgiannis. Text categorization as a graph  
 590 classification problem. In *Proceedings of the 53rd Annual Meeting of the Association for Compu-*  
 591 *tational Linguistics and the 7th International Joint Conference on Natural Language Processing*  
 592 *(Volume 1: Long Papers)*, pp. 1702–1712, 2015.

593

594 Ida Schomburg, Antje Chang, Christian Ebeling, Marion Gremse, Christian Heldt, Gregor Huhn,  
 595 and Dietmar Schomburg. Brenda, the enzyme database: updates and major new developments.  
 596 *Nucleic acids research*, 32(suppl\_1):D431–D433, 2004.

597

598 Nino Shervashidze, Pascal Schweitzer, Erik Jan Van Leeuwen, Kurt Mehlhorn, and Karsten M Borg-  
 599 wardt. Weisfeiler-lehman graph kernels. *Journal of Machine Learning Research*, 12(9), 2011.

594 Vinesh Solanki, Patrick Rubin-Delanchy, and Ian Gallagher. Persistent homology of graph embed-  
 595 dings, 2021. URL <https://arxiv.org/abs/1912.10238>.

596

597 Petar Veličković, Guillem Cucurull, Arantxa Casanova, Adriana Romero, Pietro Lio, and Yoshua  
 598 Bengio. Graph attention networks. *arXiv preprint arXiv:1710.10903*, 2017.

599

600 Haobo Wang, Ruixuan Xiao, Yixuan Li, Lei Feng, Gang Niu, Gang Chen, and Junbo Zhao. Pico:  
 601 Contrastive label disambiguation for partial label learning. In *Proceedings of the International  
 602 Conference on Learning Representations*, 2022.

603

604 Qifan Wang, Yinwei Wei, Jianhua Yin, Jianlong Wu, Xuemeng Song, and Liqiang Nie. Dualgnn:  
 605 Dual graph neural network for multimedia recommendation. *IEEE Transactions on Multimedia*,  
 606 25:1074–1084, 2021.

607

608 Wei Wang and Min-Ling Zhang. Partial label learning with discrimination augmentation. In *Pro-  
 ceedings of the International ACM SIGKDD Conference on Knowledge Discovery & Data Min-  
 ing*, pp. 1920–1928, 2022.

609

610 Max Welling and Thomas N Kipf. Semi-supervised classification with graph convolutional net-  
 611 works. In *J. International Conference on Learning Representations (ICLR 2017)*, 2016.

612

613 Keyulu Xu, Weihua Hu, Jure Leskovec, and Stefanie Jegelka. How powerful are graph neural  
 614 networks? In *International Conference on Learning Representations*, 2018.

615

616 Yan Yan and Yuhong Guo. Mutual partial label learning with competitive label noise. In *The  
 Eleventh International Conference on Learning Representations*, 2023.

617

618 Yuning You, Tianlong Chen, Yongduo Sui, Ting Chen, Zhangyang Wang, and Yang Shen. Graph  
 619 contrastive learning with augmentations. In *Advances in Neural Information Processing Systems*,  
 2020.

620

621 Guoxian Yu, Hailong Zhu, and Carlotta Domeniconi. Predicting protein functions using incomplete  
 622 hierarchical labels. *BMC bioinformatics*, 16(1):1–12, 2015a.

623

624 Yi Yu, Tengyao Wang, and Richard J Samworth. A useful variant of the davis–kahan theorem for  
 625 statisticians. *Biometrika*, 102(2):315–323, 2015b.

626

627 Tong Zhang, Yun Wang, Zhen Cui, Chuanwei Zhou, Baoliang Cui, Haikuan Huang, and Jian Yang.  
 628 Deep wasserstein graph discriminant learning for graph classification. In *Proceedings of the AAAI  
 Conference on Artificial Intelligence*, volume 35, pp. 10914–10922, 2021a.

629

630 Zaixi Zhang, Qi Liu, Hao Wang, Chengqiang Lu, and Chee-Kong Lee. Motif-based graph self-  
 631 supervised learning for molecular property prediction. *Advances in Neural Information Process-  
 ing Systems*, 34:15870–15882, 2021b.

632

633

634

635

636

637

638

639

640

641

642

643

644

645

646

647

648 **A PROOF OF THEOREM 1**  
649

650 To begin with, we denote adjacent matrix of graph  $i$  as  $A^{(i)}$  for the sake of convenience, take  
651 READOUT function as the mean in (2) that  $g_i = \frac{1}{|\mathcal{V}_i|} \sum_{v \in \mathcal{V}_i} h_v^{(i)}$ . Since  $p_c$  is the prototype of  
652 label  $c$ , we assume the latent representations of nodes satisfy  
653

654 
$$\mathbb{E} [h_v^{(i)} | y_i^* = c] = p_c, \forall v \in \mathcal{V}_i. \quad (20)$$
  
655

656 where  $y_i^*$  is the ground-truth label of graph  $i$ . Assume the latent representations of nodes in one  
657 graph are identically distributed, it follows from (20) and the law of large number that for any graph  
658  $i$  with true label  $y_i^* = c$ 

659 
$$g_i = \frac{1}{|\mathcal{V}_i|} \sum_{v \in \mathcal{V}_i} h_v^{(i)} \xrightarrow{a.s.} \mathbb{E} [h_v^{(i)} | y_i^* = c] = p_c$$
  
660

661 as  $|\mathcal{V}_i| \rightarrow \infty$ , which is account for (3) to a certain degree. As for the adjacent matrix, we refer to (Gu  
662 et al., 2024) to consider the generalized random dot product graph, which can date back to (Solanki  
663 et al., 2021) that for graph  $i$ :

664 
$$\mathbb{P} (A_{jk}^{(i)} = 1 | \Theta) = \alpha_n \xi_j^T I_{r,-r} \xi_k$$
  
665

666 where  $\Theta = (\xi_1, \dots, \xi_n) \sim F^{(i)}$ ,  $I_{r,-r} = \text{diag}(I_r, -I_r)$ . We assume the distribution  $F^{(i)}$  is deter-  
667 mined by the global graph feature  $g_i$  that there exist a continuous matrix function  $\mathcal{M}$  such that

668 
$$A^{(i)} = \mathcal{M}(g_i), \forall i \in \{1, 2, \dots, N\}. \quad (21)$$
  
669

670 Take coefficients  $\alpha_{vc}^{(i)} = \frac{1}{|\mathcal{V}_i|}$  and denote  $\lambda_p^{(i)}, u_p^{(i)}$  as the  $p$ -th eigenvalue, eigenvector for graph  $i$  for  
671 the sake of simplicity. First we consider if  $y_i^* = c, y_j^* = c'$  then by (20) and the continuity theorem

672 
$$\begin{aligned} \cos(r_i^{(c)}, r_j^{(c')}) &= \sum_{v \in \mathcal{V}_i, v' \in \mathcal{V}_j} \alpha_{vc}^{(i)} \alpha_{v'c'}^{(j)} \cos(h_v^{(i)}, h_{v'}^{(j)}) \\ &= \cos\left(\sum_{v \in \mathcal{V}_i} \frac{1}{|\mathcal{V}_i|} h_v^{(i)}, \frac{1}{|\mathcal{V}_j|} \sum_{v' \in \mathcal{V}_j} h_{v'}^{(j)}\right) \xrightarrow{a.s.} \cos(p_c, p_{c'}) \end{aligned}$$
  
673

674 as  $|\mathcal{V}_i|, |\mathcal{V}_j| \rightarrow \infty$ , and

675 
$$\cos(r_i^{(c)}, p_c) = \sum_{v \in \mathcal{V}_i} \alpha_{vc}^{(i)} \cos(h_v^{(i)}, p_c) = \cos\left(\frac{1}{|\mathcal{V}_i|} \sum_{v \in \mathcal{V}_i} h_v^{(i)}, p_c\right) \xrightarrow{a.s.} \cos(p_c, p_c) = 1,$$
  
676

677 as  $|\mathcal{V}_i| \rightarrow \infty$ , which further implies

678 
$$\begin{aligned} \mathbb{P}(A_{ij}^{spa} = 1 | y_i^* = y_j^*) &= \sum_{c=1}^C \mathbb{P}(A_{ij}^{spa} = 1 | y_i^* = y_j^* = c) \mathbb{P}(y_i^* = y_j^* = c | y_i^* = y_j^*) \\ &\geq \sum_{c=1}^C \mathbb{P}(s_{ij}^{spa} = 1 | y_i^* = y_j^* = c) \mathbb{P}(y_i^* = y_j^* = c | y_i^* = y_j^*) \\ &\geq \sum_{c=1}^C \mathbb{P}\left(\cos(r_i^{(c)}, r_j^{(c)}) = \cos\left(\frac{r_i^{(c)} + r_j^{(c)}}{2}, p_c\right) = 1 | y_i^* = y_j^* = c\right) \mathbb{P}(y_i^* = y_j^* = c | y_i^* = y_j^*) \\ &\rightarrow \sum_{c=1}^C \mathbb{P}(y_i^* = y_j^* = c | y_i^* = y_j^*) = 1, \end{aligned}$$
  
679

680 as  $|\mathcal{V}_i|, |\mathcal{V}_j| \rightarrow \infty$ , where the second and third line follow from the definitions of  $A^{spa}$  and  $s_{ij}^{spa}$ . As  
681 for (12), observe that (21) indicates the adjacent matrix of graph  $i$  given  $y_i^* = c$  satisfies

682 
$$A^{(i)} = \mathcal{M}\left(\frac{1}{|\mathcal{V}_i|} \sum_{v \in \mathcal{V}_i} h_v^{(i)}\right) \xrightarrow{a.s.} \mathcal{M}(p_c)$$
  
683

702 as  $|\mathcal{V}_i| \rightarrow \infty$ , which implies  $\|A^{(i)} - A^{(j)}\|_F \xrightarrow{a.s.} 0$  given  $y_i^* = y_j^* = c$ . Further by Weyl's  
703 Perturbation Theorem in (Oudghiri, 2005) we have

$$704 \quad 705 \quad \left| \lambda_p^{(i)} - \lambda_p^{(j)} \right| \leq \|A^{(i)} - A^{(j)}\|_F \xrightarrow{a.s.} 0,$$

706 while by a variant of Davis-Kahan Theorem, Theorem 2 in (Yu et al., 2015b) and  
707  $\min_{1 \leq i \leq N, 1 \leq p \leq T} \left| \lambda_{p+1}^{(i)} - \lambda_p^{(i)} \right| \geq \delta$  we have  
708

$$709 \quad 710 \quad \|u_p^{(i)} - u_p^{(j)}\| \leq \frac{4}{\delta} \|A^{(i)} - A^{(j)}\|_F \xrightarrow{a.s.} 0$$

711 for  $1 \leq p \leq T$ . Therefore by (8) and the continuity theorem we have

$$712 \quad \|z_i^{(p)} - z_j^{(p)}\| \xrightarrow{a.s.} 0$$

713 for  $1 \leq p \leq T$ , which leads to

$$714 \quad 715 \quad 1 \geq \cos \left( z_i^{(p)}, z_j^{(p)} \right) = \frac{\|z_i^{(p)}\|^2 + \|z_j^{(p)}\|^2 - \|z_i^{(p)} - z_j^{(p)}\|^2}{2\|z_i^{(p)}\| \cdot \|z_j^{(p)}\|} \xrightarrow{a.s.} \frac{\|z_i^{(p)}\|^2 + \|z_j^{(p)}\|^2}{2\|z_i^{(p)}\| \cdot \|z_j^{(p)}\|} \geq 1.$$

716 Then by the definitions of  $A^{spe}$  and  $s_{ij}^{spe}$  we obtain

$$717 \quad 718 \quad \mathbb{P}(A_{ij}^{spe} = 1 | y_i^* = y_j^*) = \sum_{c=1}^C \mathbb{P}(A_{ij}^{spe} = 1 | y_i^* = y_j^* = c) \mathbb{P}(y_i^* = y_j^* = c | y_i^* = y_j^*) \\ 719 \quad 720 \quad \geq \sum_{c=1}^C \mathbb{P}(s_{ij}^{spe} = 1 | y_i^* = y_j^* = c) \mathbb{P}(y_i^* = y_j^* = c | y_i^* = y_j^*) \\ 721 \quad 722 \quad \geq \sum_{c=1}^C \mathbb{P}(\cos(z_i^{(p)}, z_j^{(p)}) = 1, p = 1, \dots, T | y_i^* = y_j^* = c) \mathbb{P}(y_i^* = y_j^* = c | y_i^* = y_j^*) \\ 723 \quad 724 \quad \rightarrow \sum_{c=1}^C \mathbb{P}(y_i^* = y_j^* = c | y_i^* = y_j^*) = 1,$$

730 as  $|\mathcal{V}_i|, |\mathcal{V}_j| \rightarrow \infty$ , which completes the proof.  $\square$

## 732 B PROOF OF THEOREM 2

734 Recall that we assume the classifier is well-trained such that

$$735 \quad 736 \quad f_{\text{classifier}}(p_c) = \mathbb{I}_c, \forall c \in \mathcal{Y}, \quad (22)$$

737 where  $\mathbb{I}_c \in \{0, 1\}^C$  denotes one-hot vector whose  $c$ -th component is 1 and the rest are 0. By  
738 Theorem 1 and (13) we have

$$739 \quad 740 \quad Y_i^{(T)} \xrightarrow{a.s.} Y_i^*$$

741 as  $|\mathcal{V}_i|, T \rightarrow \infty$ , which further implies  $Q_i \xrightarrow{a.s.} Y_i^*$  according to (15). By the continuity theorem  
742 and (22) we have

$$743 \quad 744 \quad P_i = f_{\text{classifier}}(g_i) = f_{\text{classifier}} \left( \sum_{v \in \mathcal{V}_i} \frac{1}{|\mathcal{V}_i|} h_v^{(i)} \right) \rightarrow f_{\text{classifier}}(p_{y_i^*}) = \mathbb{I}_{y_i^*} = Y_i^* \quad (23)$$

745 as  $|\mathcal{V}_i| \rightarrow \infty$ . Denote  $|\mathcal{V}| = \min_{1 \leq i \leq N} |\mathcal{V}_i|$ , by dominated convergence theorem and (16) we obtain

$$746 \quad 747 \quad \lim_{|\mathcal{V}|, T \rightarrow \infty} \mathbb{E}[\mathcal{L}_{sup}] = -\frac{1}{B} \sum_{i=1}^B \lim_{|\mathcal{V}|, T \rightarrow \infty} \mathbb{E} \left[ \log \sum_{c \in S_i} \text{Softmax}(P_i)_c \cdot Q_{ic} \right] \\ 748 \quad 749 \quad = -\frac{1}{B} \sum_{i=1}^B \mathbb{E} \left[ \lim_{|\mathcal{V}|, T \rightarrow \infty} \log \left( \sum_{c \neq y_i^*} \text{Softmax}(P_i)_c \cdot Q_{ic} + (P_i)_{y_i^*} \cdot Q_{i, y_i^*} \right) \right] \\ 750 \quad 751 \quad = -\frac{1}{B} \sum_{i=1}^B \mathbb{E} \log [0 + 1] = 0$$

752 where the last line follows from (18) and (23).  $\square$

756 C RELATED WORK  
757758 C.1 GRAPH CLASSIFICATION  
759

760 Graph classification has been widely applied in fields such as molecular property prediction, protein  
761 interaction analysis, and social network modeling (Fang et al., 2022; Wang et al., 2021). Traditional graph kernel methods (Shervashidze et al., 2011) measure structural similarity through sub-  
762 graph comparisons, but scale poorly to large graphs. Recent advances in Graph Neural Networks  
763 (GNNs) (Welling & Kipf, 2016; Hamilton et al., 2017; Veličković et al., 2017; Xu et al., 2018) have  
764 shown superior performance by aggregating local neighborhood information and generating graph-  
765 level representations via pooling operators (Lee et al., 2019; Gao & Ji, 2019; Lee et al., 2021).  
766 Spectral approaches like EigenMLP (Bo et al., 2023) provide an alternative by encoding global  
767 graph structure through Fourier-like eigenvalue embeddings. Despite their success, these methods  
768 heavily rely on clean and abundant labels, which are often unavailable in real-world scenarios due  
769 to annotation cost or inherent uncertainty. While self-supervised methods such as GraphCL (You  
770 et al., 2020) avoid labels during pre-training, they still require accurate annotations for downstream  
771 classification and tend to degrade significantly under label ambiguity. Our work takes a step further  
772 by addressing the graph classification task under partial-label settings with relational inference over  
773 spatial and spectral cues.

774 C.2 PARTIAL LABEL LEARNING  
775

776 Partial label learning (PLL) considers a weak supervision setting where each training instance is  
777 annotated with a candidate label set containing only one correct label (Hüllermeier & Beringer,  
778 2005; Cour et al., 2011). Early approaches treat all candidates equally by averaging losses, but  
779 such uniform assumptions often fail under high label ambiguity. Later works focus on disambiguation,  
780 estimating true labels through confidence-based or similarity-driven refinement (Feng & An,  
781 2019; Wang & Zhang, 2022). Recent advances introduce contrastive learning to PLL (Wang et al.,  
782 2022), where prototype-instance alignment helps separate correct labels from distractors. However,  
783 these methods are mostly designed for Euclidean data such as images or texts. On graph-structured  
784 data, PLL remains underexplored. DEER (Gu et al., 2024) is one of the few attempts, proposing  
785 to measure semantic distribution divergence between graph views for contrastive learning and using  
786 posterior-guided soft label correction. Nonetheless, DEER relies on semantic distribution matching  
787 and lacks fine-grained structural modeling. Another work, GPCD (Gao et al., 2024), introduces  
788 graph potential cause discovery to estimate causal subsets for supervision, but suffers from high  
789 training complexity and overlooks global spectral cues. In contrast, PRISM integrates spatial sub-  
790 structure information and spectral semantics into a unified relational inference framework, enabling  
791 more precise and robust label disambiguation under complex graph structures.

792 D MORE EXPERIMENTAL RESULTS  
793

794 We present additional results under the low ambiguity level ( $q = 0.1, q = 0.02$ ) in Table 3. Across  
795 all datasets, PRISM consistently achieves the best performance, reaffirming its robustness under  
796 mild supervision noise. In particular, clear gains are observed on fine-grained datasets such as  
797 COIL-DEL, where both spatial and spectral cues play a pivotal role in resolving semantic ambi-  
798 guities. These results complement the main findings in Section 4.2, further demonstrating that our  
799 framework sustains strong generalization across diverse noise regimes.

800 E DETAILS OF DATASETS  
801

802 To rigorously evaluate the effectiveness of our proposed PRISM, we conduct extensive experiments  
803 on five graph classification benchmarks spanning bioinformatics and visual domains: ENZYMES,  
804 Letter-High, COIL-DEL, CIFAR10, and COLORS-3. These datasets provide a wide range of struc-  
805 tural configurations and semantic granularities, enabling a comprehensive analysis of PRISM under  
806 varied supervision conditions.

807 • **ENZYMES** (Schomburg et al., 2004) is a bioinformatics dataset comprising 600 protein tertiary  
808 structures. Each graph represents a protein, where nodes correspond to secondary structure ele-

810  
 811 Table 3: The classification accuracy (mean% $\pm$ std%) on five graph benchmark datasets. The best  
 812 results are shown in boldface and the second best results are underlined.  $q = P(\bar{y} \in Y | \bar{y} \neq y)$   
 813 reflecting the degree of label ambiguity.

Dataset	ENZYMES	Letter-High	COIL-DEL	CIFAR10	COLORS-3
Methods	$q = 0.1$	$q = 0.1$	$q = 0.02$	$q = 0.1$	$q = 0.1$
GCN	$61.33 \pm 2.85$	$50.09 \pm 0.70$	$60.77 \pm 1.71$	$47.18 \pm 1.09$	$90.34 \pm 0.06$
GAT	$58.22 \pm 3.03$	$73.39 \pm 1.41$	$69.11 \pm 2.86$	$57.56 \pm 0.65$	$89.33 \pm 1.42$
GIN	$59.78 \pm 4.58$	$55.83 \pm 4.28$	$55.94 \pm 1.69$	$47.29 \pm 0.61$	$63.01 \pm 1.45$
GraphSAGE	$60.89 \pm 1.09$	$78.20 \pm 1.17$	$71.40 \pm 2.15$	$57.22 \pm 0.67$	$91.70 \pm 2.18$
TopKPool	$53.11 \pm 4.12$	$67.07 \pm 1.60$	$55.80 \pm 4.86$	$55.26 \pm 0.85$	$82.35 \pm 1.36$
SAGPool	$56.89 \pm 5.37$	$67.42 \pm 1.91$	$52.94 \pm 2.59$	$54.23 \pm 0.53$	$76.99 \pm 4.39$
EdgePool	$58.67 \pm 2.67$	$70.49 \pm 3.29$	$68.74 \pm 1.85$	$55.09 \pm 0.61$	$87.47 \pm 0.41$
ASAP	$60.89 \pm 2.67$	$71.25 \pm 1.44$	$59.03 \pm 3.09$	$54.56 \pm 0.66$	$77.84 \pm 1.26$
Graph Transplant	$61.56 \pm 2.86$	$80.75 \pm 0.60$	$80.09 \pm 0.75$	$56.87 \pm 1.28$	$85.48 \pm 0.89$
PiCO	$61.08 \pm 6.67$	$81.27 \pm 1.60$	$84.88 \pm 1.09$	$57.70 \pm 0.82$	$65.68 \pm 1.07$
TGNN	$62.44 \pm 3.01$	$78.55 \pm 0.78$	$70.49 \pm 0.87$	OOM	$93.16 \pm 1.55$
GraphCL	$61.78 \pm 1.51$	$78.43 \pm 0.85$	$78.83 \pm 1.06$	$57.62 \pm 0.56$	$92.71 \pm 1.61$
GraphACL	$58.22 \pm 1.51$	$81.04 \pm 1.01$	$80.66 \pm 0.41$	$57.65 \pm 0.21$	$92.05 \pm 0.50$
DEER	$67.11 \pm 1.66$	$83.48 \pm 0.92$	$87.86 \pm 1.41$	$61.45 \pm 0.40$	$96.23 \pm 2.94$
<b>PRISM (Ours)</b>	<b><math>68.00 \pm 1.63</math></b>	<b><math>84.87 \pm 0.74</math></b>	<b><math>89.29 \pm 1.36</math></b>	<b><math>61.73 \pm 0.87</math></b>	<b><math>98.36 \pm 1.07</math></b>

830  
 831 ments (e.g., helices, strands), and edges indicate either spatial proximity or sequential adjacency.  
 832 The classification involves assigning one of six enzyme commission (EC) classes.

- 833 • **Letter-High** (Riesen & Bunke, 2008) contains graphs constructed from 15 uppercase letters. Each  
 834 letter is transformed into a prototype graph by representing stroke endpoints as nodes and line  
 835 segments as edges. The dataset emphasizes shape topology and inter-class similarity among char-  
 836 acters.
- 837 • **COIL-DEL** (Riesen & Bunke, 2008) is derived from object images by applying Harris corner  
 838 detection followed by Delaunay triangulation. This results in undirected graphs where nodes  
 839 denote detected corners and edges reflect geometric connectivity. The dataset includes 100 object  
 840 categories with significant structural variation.
- 841 • **CIFAR10** (Dwivedi et al., 2020) is constructed from an image classification benchmark by trans-  
 842 forming each image into a graph representation based on superpixels. In this formulation, nodes  
 843 denote individual superpixels, and edges are established according to  $k$ -nearest neighbor rela-  
 844 tionships. The dataset further exhibits a hierarchical taxonomy: the first super-class (*vehicles*)  
 845 comprises airplane, automobile, ship, and truck (excluding pickup truck), whereas the second  
 846 super-class (*animals*) encompasses bird, cat, deer, dog, frog, and horse.
- 847 • **COLORS-3** (Knyazev et al., 2019) is a synthetic benchmark for evaluating reasoning over discrete  
 848 node attributes. Each graph contains nodes with categorical color features (red, green, blue),  
 849 encoded as one-hot vectors. The task is to count the number of nodes of a specified color, requiring  
 850 models to identify and aggregate attribute-specific information.

851  
 852 To emulate the partial-label learning scenario, we adopt the controlled label corruption protocol  
 853 in (Gu et al., 2024), wherein each sample is provided with a candidate label set that includes the  
 854 ground-truth label and randomly sampled distractors. The inclusion probability  $q = P(\bar{y} \in \mathcal{S}_i |$   
 855  $\bar{y} \neq y_i)$  determines the ambiguity level of the candidate supervision. We set  $q \in \{0.1, 0.3, 0.5\}$   
 856 for ENZYMES, Letter-High, and COLORS-3, while smaller values  $\{0.02, 0.05, 0.1\}$  are chosen for  
 857 COIL-DEL due to its larger label space and increased visual complexity.

## 858 F DETAILS OF BASELINES

861  
 862 We compare our proposed PRISM against a broad spectrum of baseline models categorized into  
 863 seven distinct groups: (a) *Graph neural networks*: GCN (Welling & Kipf, 2016), GAT (Veličković  
 864 et al., 2017), GIN (Xu et al., 2018), and GraphSAGE (Hamilton et al., 2017); (b) *Hierarchical graph*  
 865 *pooling*: TopKPool (Gao & Ji, 2019), SAGPool (Lee et al., 2019), EdgePool (Diehl, 2019), and

864 ASAP (Ranjan et al., 2020) (all using GraphSAGE as the encoder backbone); (c) *Graph augmentation method*: Graph Transplant (Park et al., 2022); (d) *Contrastive graph learning*: GraphCL (You  
 865 et al., 2020) and GraphACL (Luo et al., 2023); (e) *Weakly-supervised learning*: TGNN (Ju et al.,  
 866 2023); (f) *Partial-label learning in vision*: PiCO (Wang et al., 2022), adapted with a GraphSAGE  
 867 encoder; (g) *Partial-label learning for graphs*: DEER (Gu et al., 2024), which operates directly on  
 868 the partial supervision scenario. These baselines span diverse learning paradigms and offer comple-  
 869 mentary modeling assumptions, providing a comprehensive testbed for evaluation.

870

- 871 • **GCN** (Welling & Kipf, 2016): A spectral convolutional network that leverages renormalized ad-  
 872 jacency matrices to aggregate first-order neighborhood information in a computationally efficient  
 873 manner.
- 874 • **GAT** (Veličković et al., 2017): Introduces attention weights over neighbors, enabling each node to  
 875 prioritize important neighbors during message passing.
- 876 • **GIN** (Xu et al., 2018): Uses MLPs to approximate injective functions over multisets of neighbors,  
 877 achieving powerful discriminative capacity aligned with the Weisfeiler-Lehman graph test.
- 878 • **GraphSAGE** (Hamilton et al., 2017): Aggregates information from randomly sampled neighbors  
 879 and generalizes to unseen graphs via inductive learning, making it scalable to large datasets.
- 880 • **TopKPool** (Gao & Ji, 2019): Selects top-ranked nodes based on a learnable projection score to  
 881 form a pooled graph with reduced size and preserved discriminative regions.
- 882 • **SAGPool** (Lee et al., 2019): Utilizes self-attention scores computed from graph convolutions to  
 883 guide node selection for pooling, capturing both feature and structural signals.
- 884 • **EdgePool** (Diehl, 2019): Contracts informative edges iteratively to coarsen the graph while main-  
 885 taining crucial topological structures.
- 886 • **ASAP** (Ranjan et al., 2020): Combines node selection and clustering by learning soft assignments  
 887 over local  $h$ -hop neighborhoods, allowing for adaptive structure-aware pooling.
- 888 • **Graph Transplant** (Park et al., 2022): A mixup-inspired data augmentation strategy that extracts  
 889 meaningful subgraphs based on node saliency and generates hybrid samples through substructure-  
 890 level interpolation.
- 891 • **GraphCL** (You et al., 2020): A contrastive learning framework that maximizes agreement be-  
 892 tween different augmented views of a graph, using stochastic transformations and InfoNCE loss.
- 893 • **GraphACL** (Luo et al., 2023): Improves contrastive representation learning by constructing ad-  
 894 versarial hard negatives and regularizing the feature space with orthogonality and divergence con-  
 895 straints.
- 896 • **TGNN** (Ju et al., 2023): A dual-view semi-supervised framework that integrates message passing  
 897 and kernel-based reasoning, encouraging consistency across views to exploit both labeled and  
 898 unlabeled graphs.
- 899 • **PiCO** (Wang et al., 2022): Learns a set of class-wise prototypes and employs contrastive objec-  
 900 tives to align instance embeddings with their correct prototypes. We adopt a GraphSAGE encoder  
 901 to enable graph-level application.
- 902 • **DEER** (Gu et al., 2024): A partial-label graph learning method that selects reliable positive pairs  
 903 by measuring distribution divergence across augmented views. It also performs soft label cor-  
 904 rection via posterior estimation. However, it does not explicitly model substructures or spectral  
 905 signals, limiting its granularity in structural reasoning.

906 **Training Protocol.** All baselines are trained under partial-label supervision using a cross-entropy  
 907 loss over candidate label sets. TGNN additionally optimizes a consistency loss between dual views.  
 908 For contrastive methods such as GraphCL and PiCO, we apply their contrastive loss and the cross-  
 909 entropy loss. Pooling-based methods are evaluated with a fixed reduction ratio of 0.6 and use Graph-  
 910 SAGE as their encoder. All models are trained under identical random seeds for controlled compar-  
 911 isons.

## 912 G DETAILS OF IMPLEMENTATION

913  
 914 We implement all models using PyTorch with the PyG backend. A two-layer GraphSAGE with 512  
 915 hidden units is adopted as the shared encoder. The model is trained using the Adam optimizer with a

918 learning rate of 0.001 and a batch size of 128. The EMA momentum for prototype and label updates  
919 is set to  $m = 0.99$ , and the propagation momentum is  $\alpha = 0.9$  with  $T = 2$  steps. Both spatial and  
920 spectral relational graphs connect each graph to  $k_a = k_e = 5$  neighbors. Eigen-decomposition is  
921 precomputed via sparse solvers to ensure efficiency. For ENZYMES, Letter-High, COIL-DEL, and  
922 COLORS-3, we partition the data into training, validation, and test sets with a ratio of 80%:5%:15%.  
923 For CIFAR10, we adopt the conventional split of 45,000 training, 5,000 validation, and 10,000 test  
924 graphs, consistent with the protocol in (Dwivedi et al., 2020). All reported results are averaged over  
925 five independent random seeds.

## 927 LLMs USAGE

929 We adhere to the ICLR Code of Ethics. We use large language models solely for polishing writing.  
930 All scientific contributions remain entirely our own.

931  
932  
933  
934  
935  
936  
937  
938  
939  
940  
941  
942  
943  
944  
945  
946  
947  
948  
949  
950  
951  
952  
953  
954  
955  
956  
957  
958  
959  
960  
961  
962  
963  
964  
965  
966  
967  
968  
969  
970  
971